

Low Complexity Adaptive Beamformer for Active Sonar Imaging



Jo Inge Buskenes, Roy Edgar Hansen, Andreas Austeng

Abstract—We have studied the low complexity adaptive (LCA) beamformer in active sonar imaging. LCA can be viewed as either a simplification of the minimum variance distortionless response (MVDR) beamformer, or as an adaptive extension to the delay and sum (DAS) beamformer. While both LCA and MVDR attempt to minimize the power of noise and interference in the image, MVDR seeks the optimal solution by estimating and inverting the array's spatial covariance matrix, while LCA selects the best performer from a predefined set of sensor windows.

We show that a robust MVDR implementation typically creates responses ranging between that of the rectangular and Hamming. We let LCA select from a set of Kaiser windows with responses in this range, and add some steered variations of each. We limit the steering to roughly half the -3 dB width of the window's amplitude response. Using experimental data from the Kongsberg Maritime HISAS 1030 sonar we find that LCA and MVDR produce nearly identical images of large scenes, both being superior to DAS. On point targets LCA is able to double the resolution compared to DAS, or provide half that of MVDR. This performance is achieved with a total of 6 windows; the rectangular and Kaiser window with $\beta = 5$, in unsteered version, and left and right steered to the steering limit. Slightly smoother images are produced if the window count is increased to 15, but past this we observe minimal difference. Finally we show that LCA work just as well if Kaiser windows are substituted with trigonometric ones.

All our observations and experiences point to LCA being very easy to manage. It simply works, and is surprisingly insensitive to the exact type of window function, steering amount, or number of windows. It can be efficiently implemented on parallel hardware, and handles any scene without the need for parameter adjustments.

Index Terms—Beamforming, adaptive beamforming, MVDR, LCA, sonar, active, complexity.

I. INTRODUCTION

THE best adaptive sonars are found in nature. Bats, for instance, use a high frequency sonar to detect, identify and track prey with amazing precision in caves amongst a myriad of other bats. Active human made sonars have little to no adaptability on transmit, but several adaptive methods have been investigated post process the received data. Perhaps the best studied method for reconstructing a sonar image is the minimum variance distortion-less response (MVDR) beamformer [1]. It adapts the sonar array's response to minimize the influence of noise and interference in the final image.

In many cases MVDR can improve the contrast and resolution of active sonar images compared to conventional static

All authors are with the Department of Informatics, University of Oslo, Norway.

R. E. Hansen is also with the Norwegian Defense Research Establishment (FFI), Norway.

methods [2]–[5]. However, while the computational complexity of conventional beamformers are linear with the number of channels, $O(M)$, MVDR is at $O(M^3)$. This makes MVDR impracticable and sometimes infeasible. We have shown in previous studies that MVDR's complexity can be reduced, and its implementation accelerated significantly using graphics computing units (GPUs) [6], [7]. However, while MVDR relies on estimating and inverting a spatial covariance matrix, there exist a method that avoid this altogether.⁽¹⁾

This method is called the Low Complexity Adaptive (LCA) beamformer. It was first proposed by Synnevåg in clinical medical imaging [8], who demonstrated its ability to obtain very similar results to MVDR in a system with focused transmit beams. LCA applies a set of predefined windows and selects the one offering the best noise suppression. It relies on the same optimization criterion as MVDR, and may be considered a version of MVDR with a reduced window solution space. Alternatively, it may be viewed as a delay-and-sum (DAS) beamformer with an adaptive extension.

Synnevåg used a window set comprised of rectangular, Kaiser and inverted Kaiser functions.⁽²⁾ He made LCA choose from 12 unique windows, 6 of which were micro-steered variants of a fairly wide Kaiser window. While achieving good results, it was not made clear how LCA performs with more or fewer windows, and how steering affects it all.

We use LCA with variations of the Kaiser window, but a comparison to using trigonometric windows will also be provided. We extend Synnevåg's work by steering all our windows and not just some, and elaborate on the type of Kaiser windows to include and the method of steering. Then the method is applied to experimental data from the 32 element Kongsberg Maritime HISAS 1030 synthetic aperture sonar (SAS), with an operating frequency of 100 kHz and transmit angle of 25°.

Our results show 23 grader på hvert mottakerelement
@ 100 kHz

fraction of the window's -3dB resolution. When letting LCA choose from Kaiser windows with similar responses, we obtain images with improved noise suppression and resolution. The resolution gain is made predictable by limiting the maximum steering to a fraction of the window's -3 dB width. Overall, LCA produces images that are similar to MVDR, but with a resolution in between that of DAS and MVDR. LCA is also inherently robust, easy to implement and fairly easy to understand.

This article is outlined as follows: In Section II we offer

¹May also be called Kaiser-Harris windows.

a gentle introduction to beamforming. Then we move on to adaptive beamforming and describe the MVDR and LCA methods III and IV, respectively. We use LCA with the Kaiser window which we describe in IV-A, explain how we steer it in IV-B, and by how much in IV-C. Finally we add some remarks on using the trigonometric window instead of Kaiser in IV-D, and of sampling considerations in IV-E. Results and discussion are provided in Section V, where we study MVDR's windows to find suitable LCA ones in V-A, assess the range of window types and steering in V-B, determine the number of windows needed in V-C, and add a note on computational complexity in V-E. Finally we conclude in VI.

II. RECEIVE BEAMFORMING

To form a sonar image we need to estimate source locations and amplitudes. For this purpose we apply a spatial bandpass filter to the backscattered wavefield data. The filter is called an array processor, or receive beamformer. The basic principle is to apply delay and weights to the sensor channels before summing them up, chosen such that signals from the location of interest are summed coherently, while other sources sum incoherently.

Assume that the wavefield has been sampled by an M element uniform linear array, and that the signal signature has been removed by a matched filter. Let $x_m[\theta, n]$ be the delayed data from the m th channel, where the θ and n is the azimuth angle and range sample of the focus point, respectively. Each angle θ will be processed independently, so to simplify notation we will assume the dependence on θ to be implicit from now on.

The output $z[n]$ of a beamformer is defined as the weighted sum of all the delayed data samples:

$$z[n] = \mathbf{w}^H[n] \mathbf{x}[n] = \begin{bmatrix} w_0[n] \\ w_1[n] \\ \vdots \\ w_{M-1}[n] \end{bmatrix}^H \begin{bmatrix} x_0[n] \\ x_1[n] \\ \vdots \\ x_{M-1}[n] \end{bmatrix}, \quad (1)$$

where w_m is the weight factor assigned to channel m . A weight set is commonly called a window or a taper function. Applying a window that trails off towards the edges improves noise suppression at the cost of reduced resolution [9]. Real windows lead to symmetric responses, while complex weights allow asymmetric responses.

Conventional beamformers all have static weights. The reference method is the delay-and-sum (DAS) beamformer, also known as the backprojection algorithm. It delays each pixel into focus, then applies a suitable window, and finally sums the data. The virtue of DAS is its simplicity, robustness to parameter errors, linear processing of the image and the ease of which it can be implemented on parallel hardware.

Adaptive beamformers are dynamic and seek to adjust the array response to better fit the incoming wavefield. This may be achieved by allowing either the weights or delays to change, or both. One of the most extensively studied of these methods is the minimum variance distortion-less response (MVDR) beamformer.

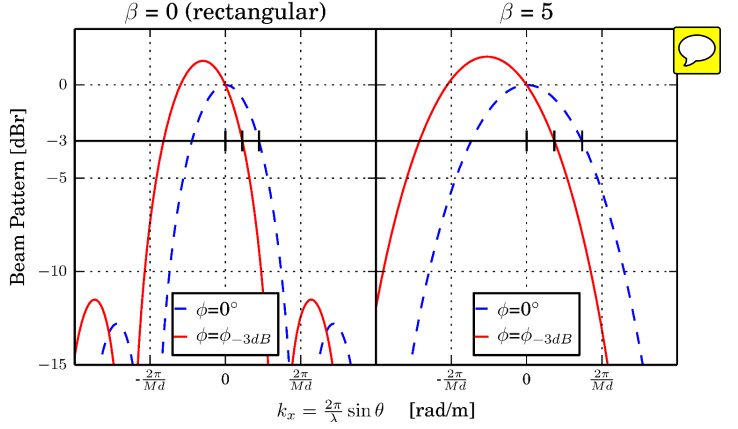


Fig. 1. Each Kaiser window is steered in the interval $\phi = [0, \phi_{3dB}(\beta)]$. The angle $\phi_{3dB}(\beta)$ is the amount of steering needed for the steered response to have a -3dB crossing that is exactly half that of the unsteered window. With each window steered this way we expect the resolution gain to remain predictable and independent of β , and we also effectively constrain the white noise gain of the beamformer.

III. MVDR

MVDR seeks to minimize the output power of the beamformer, under the constraint of a unity gain in some desired direction ϕ [1]:

$$\underset{\mathbf{w}[n]}{\operatorname{argmin}} E\{|z[n]|^2\} = \underset{\mathbf{w}[n]}{\operatorname{argmin}} \mathbf{w}[n] \mathbf{R}[n] \mathbf{w}^H[n] \quad \text{subject to } \mathbf{w}[n] \mathbf{a}_\phi = 1. \quad (2)$$

Here \mathbf{a}_ϕ is a steering vector, $E\{\cdot\}$ is the expectation operator, and $\mathbf{R}[n] = E\{\mathbf{x}\mathbf{x}^H\}$ is the spatial covariance matrix. This is a convex optimization problem with the solution:

$$\mathbf{w}[n] = \frac{\mathbf{R}^{-1}[n] \mathbf{a}_\phi}{\mathbf{a}_\phi^T \mathbf{R}^{-1}[n] \mathbf{a}_\phi}, \quad (3)$$

where $\mathbf{R} = E\{\mathbf{x}[n]\mathbf{x}^H[n]\} \in \mathbb{C}^{M,M}$ is the spatial covariance matrix for the full array. The problem lies in estimating and inverting this spatial covariance matrix. We have described the exact steps in [6]: To avoid signal cancellation we apply spatial averaging by computing a mean covariance matrix from a set of subarrays with length L [10], for true speckle statistics we perform temporal averaging over $N_k = 2K + 1$ temporal samples [11], and to improve robustness to parameter errors we add d percent diagonal loading [12], [13]. These steps are also needed to ensure that the covariance matrix is numerically well conditioned and hence invertible.

IV. LCA

A much less complex alternative to MVDR is the low complexity adaptive (LCA) beamformer. It iterates through a set of P windows and selects the window p that best fulfills the minimum variance criterion:

$$\underset{p}{\operatorname{argmin}} E\{|z_p[n]|^2\} = \underset{p}{\operatorname{argmin}} E\{|\mathbf{w}_p^H \mathbf{x}[n]|^2\} \quad \text{subject to } \mathbf{w}^H \mathbf{a}_\phi = 1. \quad (4)$$

Note how closely LCA is related to the MVDR definition in (2). The optimization criterion and constraint is the same,

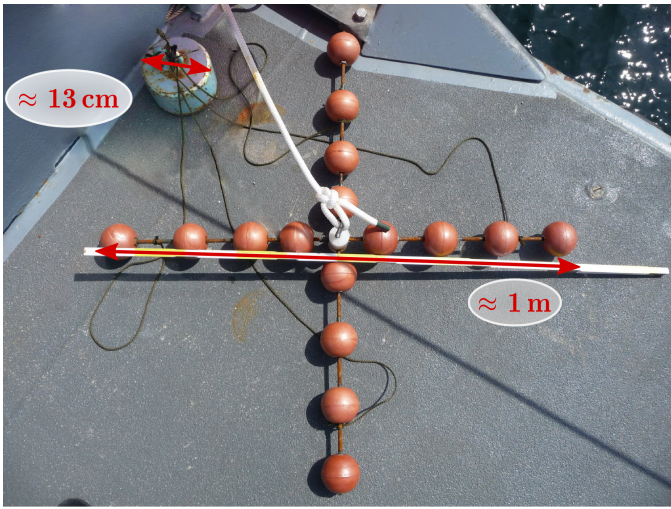


Fig. 2. One of the objects used to test the beamformers is a 1 m by 1 m cross attached to an anchor with a diameter of approximately 13 cm. Source image courtesy of Bundeswehr Technical Center for Ships and Naval Weapons, Maritime Technology and Research (WTD 71).

but LCA has a finite and discrete solution space for the weights. As will be demonstrated in section V-A, LCA will perform similarly to MVDR because a robustified MVDR implementation seems to be constrained to window functions similar to the ones we let LCA choose from.

In practice, we estimate the beamformer output power as

$$E\{|z[n]|^2\} = \frac{1}{N_k} \sum_{n'=n-K}^{n+K} |z[n']|^2$$

which computes the sample power average over $N_k = 2K + 1$ temporal samples. This is the same temporal averaging method we use for MVDR. In our case the matched filtered signal is a just few samples long, hence $K = 1$ will be used for both MVDR and LCA throughout this work.

(2) If extra flexibility is desired, we can also estimate the variance by a weighted combination of local pixels

$$E\{|z[x, n]|^2\} = \frac{1}{N_x N_k} \sum_{x'=x-X}^{x+X} \sum_{n'=n-K}^{n+K} w[x', n'] |z[x', n']|^2 \quad (5)$$

where $N_x = 2X + 1$ is the number of azimuth lines to average over, and $w_{\text{prf}}[x', n']$ is a normalized 2 dimensional weight function.

A. Window function: Kaiser

As will be demonstrated in upcoming sections, the LCA beamformer works very well with windows generated from the Kaiser-Bessel function. We will express it in vector form as:

$$\mathbf{f}_\beta = \begin{bmatrix} f_0(\beta) \\ \vdots \\ f_{M-1}(\beta) \end{bmatrix} \quad (6)$$

where

$$f_m(\beta) = \frac{I_0\left(\pi\beta\sqrt{1 - \left(\frac{2m}{M-1} - 1\right)^2}\right)}{I_0(\pi\beta)} \quad (7)$$

and I_0 is the zeroth order modified Bessel function of the first kind:

$$I_0(x) = \sum_{a=0}^{\infty} \left[\frac{(\frac{x}{2})^a}{a!} \right]^2. \quad (8)$$

The Kaiser-Bessel window is near optimal in the sense of having its peak energy concentration around $\theta = 0^\circ$, for a given time-bandwidth product specified with the parameter β :

$$\beta = \frac{TB}{2}, \quad (9)$$

where T is the extent of the window in time(3) and B is its bandwidth. Adjusting β changes the trade-off between mainlobe width and sidelobe level. When $\beta = 0$ the window becomes rectangular, while at large values ($\beta > 5$) the window converges to a Gaussian both in time and frequency. This class of windows is generally considered well suited for separating closely spaced(4) sources with amplitudes of a high dynamic range [9], they are easy to make, and they are optimal for any value of β .

Should perhaps say space-bandwidth product?

better word?

B. Steering

Adding slightly steered versions of each window to the window database gives LCA greater flexibility in searching for an optimal window. A Kaiser window \mathbf{f}_β steered to the angle ϕ can be expressed as

$$\mathbf{w}_{\beta, \phi} = \frac{\mathbf{f}_\beta^H \text{diag}(\mathbf{a}_\phi)}{\mathbf{f}_\beta^H \mathbf{a}_\phi} \quad (10)$$

where $\text{diag}(\mathbf{a}_\phi)$ is a diagonal matrix constructed from the steering vector \mathbf{a}_ϕ :

$$\mathbf{a}_\phi = \begin{bmatrix} 1 \\ e^{-j\frac{2\pi d}{\lambda} \sin(\phi)} \\ \vdots \\ e^{-j\frac{2\pi(M-1)d}{\lambda} \sin(\phi)} \end{bmatrix}. \quad (11)$$

Here d (5) is the element spacing, λ is the wavelength and ϕ is the steering amount. The normalization factor $\mathbf{f}_\beta^H \mathbf{a}_\phi$ is the reciprocal of the window's coherent gain. It ensures unit gain in the direction of interest as required by (4). Since the signal-to-noise ratio is constant for a specific window (same β -value), this normalization also proportionally increases the incoherent noise gain.

d is reused as element spacing, find an alternative

The window database we will construct will contain N_β Kaiser windows with unique β -values, each being steered in N_ϕ different directions. This gives us $N_w = N_\beta N_\phi$ unique windows.

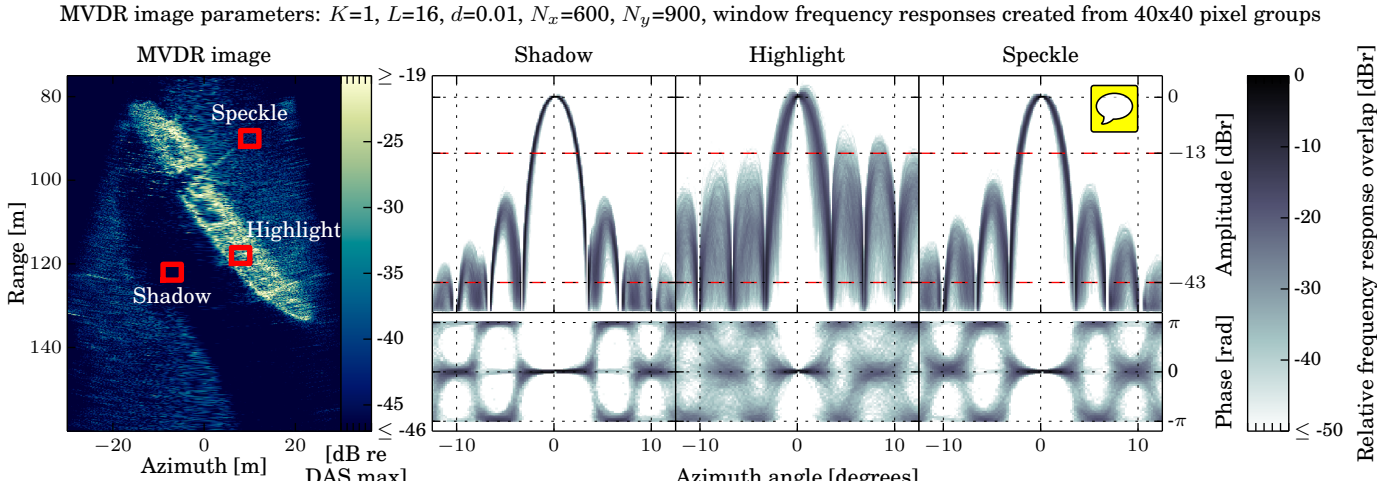


Fig. 3. Determining LCA window type: MVDR image with typical frequency responses for windows used in various pixel regions.

Left: MVDR sectorscan image of the oiltanker Holmengraa, with the pixel groups are indicated with red boxes.

Right: MVDR window amplitude and phase responses computed from 40x40 pixel groups in the shadow, highlight and speckle region of the image. The responses are overlayed each other and the amount of overlap is colored using a logarithmic scale. The dashed red lines at -13 dB and -43 dB marks the peak sidelobe levels of an unsteered rectangular and Hamming window, respectively. Note how the responses are more or less symmetric, with very little steering in the shadow, moderate steering in speckle and steering within roughly 3 dB in highlight. The phase varies most in the highlight region where we see the highest contrast.

C. Steering bounds

Each window's response is constrained to unit gain in the look direction. Hence, when it is steered the white noise gain must increase and the signal-to-noise ratio decrease, as shown in Fig. 1. To limit this we place an upper bound to the steering, chosen such that wide windows are allowed to be steered more than narrow ones. We call this upper bound for steering $\phi_{3\text{dB}}(\beta)$, and define it as the steering angle needed for the steered response to have a -3 dB crossing that is exactly half that of the unsteered window. Using a numerical search for the steering angle ϕ that fulfilled this criterion for a wide range of β -values, we obtained a third degree polynomial fit to these points:

$$\phi_{3\text{dB}}(\beta) \approx -0.002894\beta^3 + 0.02451\beta^2 - 0.01308\beta + 0.2980 \quad (12)$$

Henceforth any steering will be specified relative to this upper bound. With each window steered this way we expect the resolution gain to remain predictable and independent of β , and we also effectively constrain the white noise gain of the beamformer.

D. Trigonometric windows

While we focus on using LCA with Kaiser windows, we will for completeness compare the performance with that of using trigonometric windows. This is defined as:

$$f_m(\alpha) = \alpha - (1 - \alpha) \cos\left(\frac{2\pi m}{M - 1}\right) \quad (13)$$

where we apply the constraint $\alpha \in [0.5, 1]$ to avoid windows with negative coefficients. Steering is applied as in (10), and the α -value that halves the 3 dB distance is found using the method described in section IV-C:

$$\phi_{3\text{dB}}(\alpha) \approx -2.214\beta^3 + 6.084\beta^2 - 5.710\beta + 2.136. \quad (14)$$

E. Oversampling

The ultimate goal of adaptive beamformers is to take the information available in the field and use it to either improve image resolution, noise suppression, or both. This non-linear processing increases the image bandwidth and introduces a need for a sampling rate higher than the Nyquist rate. For MVDR a lateral oversampling factor of 10 compared to the Nyquist rate is often needed to ensure minimal spatial shift-variance in source amplitude [14].

Since LCA operates with the same optimization criterion as MVDR, we will be using approximately a factor 8 lateral oversampling for both beamformers. The images appear more visually pleasing and detailed up to 8. We consider an absolute minimum to be 2, due to the non-linear nature of delaying pixels that isn't strictly in the far field, and of displaying the absolute value of the pixels on a decibel scale. In Media Movie 1 we visualize the effect of changing the lateral oversampling factor on a set of LCA images. Upon display the images are all bilinearly upinterpolated to the same size.

V. RESULTS AND DISCUSSION

To test the performance of the MVDR and LCA beamformers, we have processed data acquired by the Kongsberg Maritime HUGIN AUV carrying their 32 element HISAS1030 sonar [15]. It is a high resolution synthetic aperture sonar with 1.2 m array length, 100 kHz operating frequency, 40 kHz bandwidth and 25° opening angle on transmission.

Two different scenes will be studied. One of the 1500 DWT oil tanker wreck Holmengraa lying at a slanted seabed at 77 m depth outside of Horten, Norway [16]. It measures 68 m by 9 m and fills most of the highlighted sector. This data was collected by the Norwegian Defense Research Establishment and Kongsberg Maritime. The other scene is of an 1 m by 1 m iron cross, connected to a an anchor with 13 cm diameter

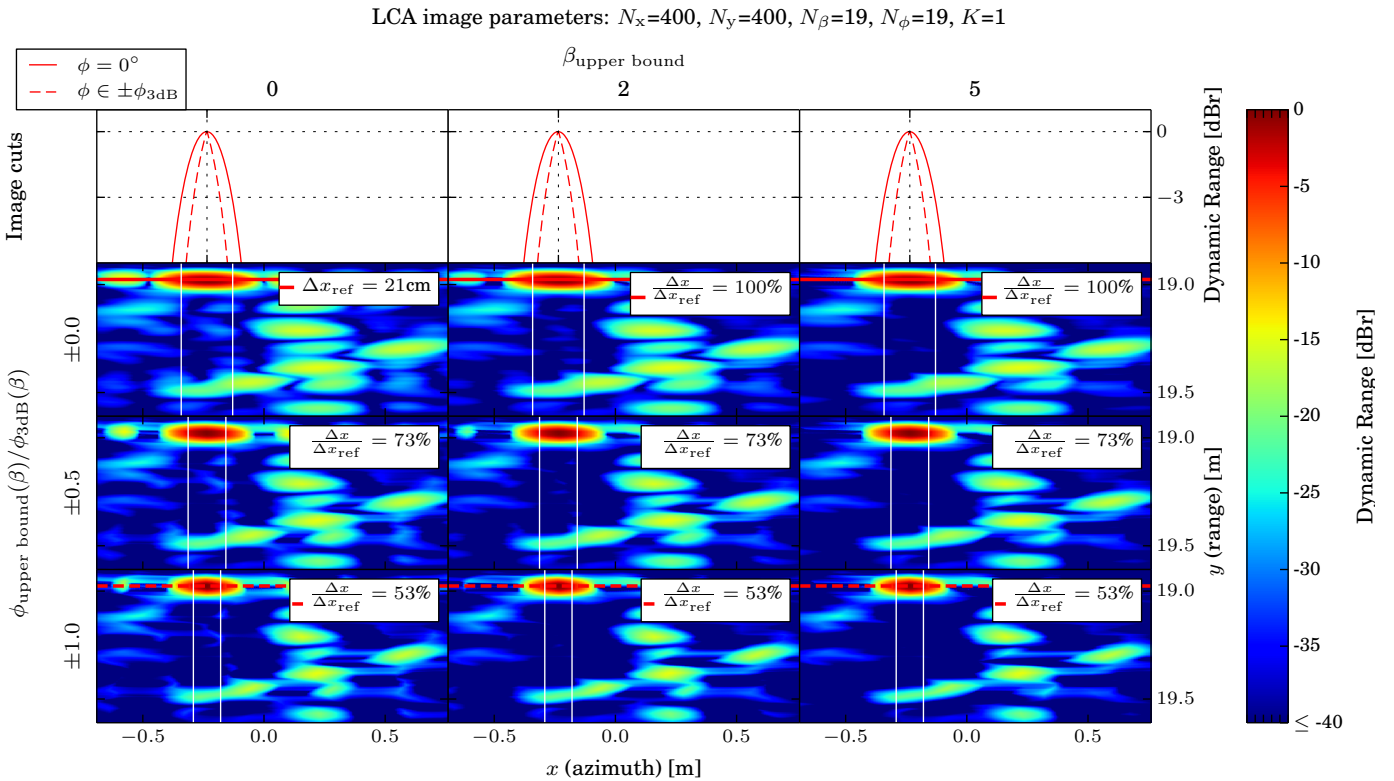


Fig. 4. *Determining Kaiser parameter boundaries:* LCA images created with a large and equal size window database, but where the upper bounds for β and ϕ varied. The upper left image is equal to DAS with a rectangular window. For all images we measure the lateral distance Δx between the two -3dB points anchor. These are specified relatively to the reference distance Δx_{ref} from the upper left DAS image.

Upper bound β : Observe that LCA gets better at suppressing sidelobes in the image as we increase the upper bounds for β . Fig. 3 suggests that MVDR tend to choose windows with levels lower than that of Kaiser with $\beta = 2$, but here we observe further improvement going to $\beta = 5$.

Upper bound ϕ : As we increase the upper bound of the steering ϕ , we also increase the lateral image resolution.

(Fig. 2). This data was collected by the Bundeswehr Technical Center for Ships and Naval Weapons, Maritime Technology and Research (WTD 71). Both scenes are imaged in sectorscan mode.

In the image reconstruction we have run MVDR with subarray length $L = 16$ and $d = 1\%$ diagonal loading(6). Both MVDR and LCA was run with $K = 1$ temporal averaging. This is a fairly aggressive yet stable set of parameters.(7)

The results will be presented in the following order: In section V-A we discuss typical window responses computed by MVDR, and hypothesize that these can be mimicked by Kaiser windows. In section V-B we determine sensible boundaries for the Kaiser parameter β and window steering ϕ . In section V-C we discuss how many window variations are needed for LCA to perform well.

A. LCA window function

Assuming that a robust MVDR is the reference method we want LCA to perform similarly to it seems sensible to create a window database for LCA with responses similar to the ones that MVDR computes. We study this in Fig. 3, where we present the typical amplitude and phase responses that MVDR creates for shadow, speckle and highlight regions of the Holmengraa scene.

Observe from Fig. 3 that MVDR seems to prefer symmetric window responses, even if it is free to choose non-symmetric

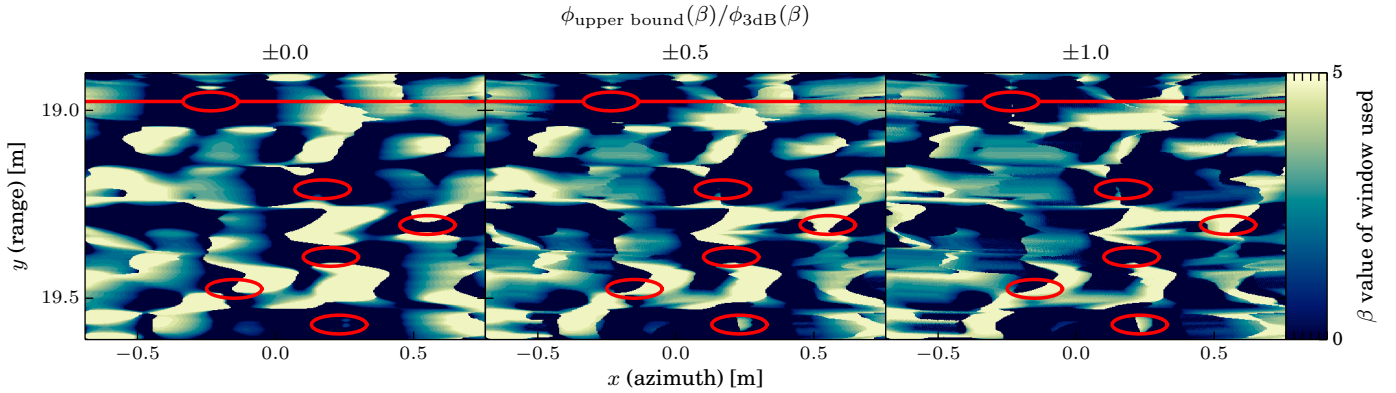
ones. The symmetry is most predominant in shadow and speckle regions, while in highlight the windows are approximately symmetric within the illuminated sector of the seafloor. We have observed this symmetry to be a side-effect of the averaging steps needed to build the sample covariance matrix, which are required for MVDR to operate in near snapshot mode in an active system. The peak sidelobe levels of the MVDR windows are mostly between -13 dB and -43 dB. This corresponds to that of an unsteered rectangular and Hamming window, or an unsteered Kaiser window with $\beta = 0$ and $\beta = 2$, respectively.

From this we hypothesize that a good window database LCA can be made using a varied set of Kaiser windows. If they span a suitable range of β -values, and some steering variations are applied to each, we should have responses that resemble those in Fig. 3. The Kaiser window is easy to compute, is fairly insensitive to coefficient inaccuracies, and can create windows with shapes spanning from rectangular to Gaussian. It is also optimal in the sense of having its peak power concentration near the steering angle.

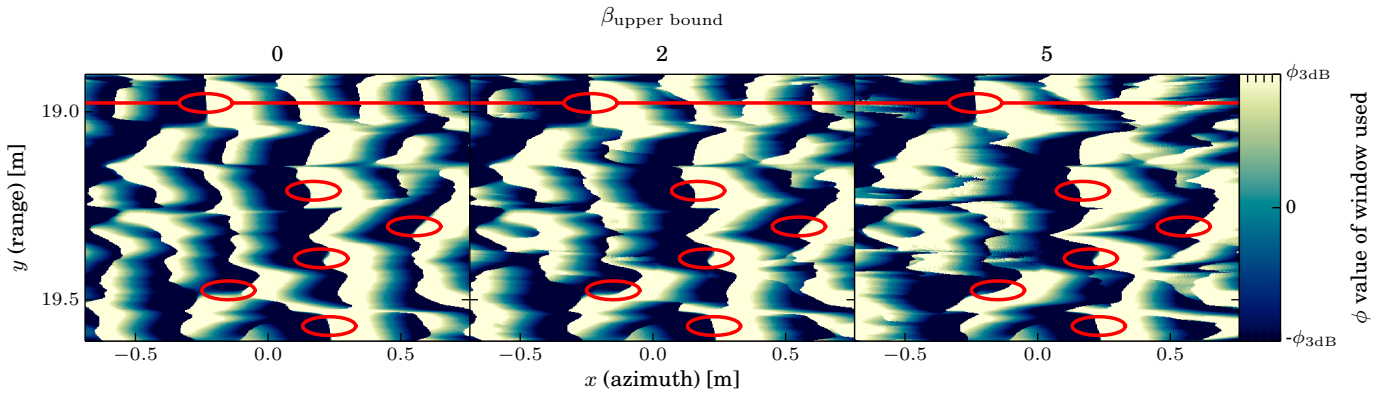
Unlike the method described by Synnevåg [8] we do not let LCA choose from inverted Kaiser windows. These have a mainlobe width narrower than that of the rectangular window, but at the expense of a very poor white noise gain. We have found that these windows hardly ever get used on experimental data, in particular steered versions of them. We can infer the

6
also used
for element
distance

7
suitable
ref?



(a) β -values of the Kaiser window chosen for each image pixel. Note how LCA prefers a narrow response ($\beta = 0$) on the anchor, and on other strong sources with little lateral interference. On the sources where lateral interference is present it chooses the widest response with the best sidelobe suppression.



(b) ϕ -values of the Kaiser window chosen for each image pixel. On strong sources LCA selects windows that are steered away from the source. This is what improves the FWHM measurement in Fig. 4.

Fig. 5. Kaiser windows chosen for each pixel in the image. The underlying image is the one shown in Fig. 4, with the same parameters. The location of the anchor, cut line and main scatter locations of the cross is marked in red.

same from Fig. 3 by noting that the maximum sidelobe level rarely exceeds the rectangular window level of -13 dB.

Media Movie 2 animates how Fig. 3 changes as a function of the MVDR subarray length L and temporal averaging K . At $L = 1$ the window responses are rectangular in all areas in the image. At $L = 2$ we observe window responses with slight amplitude variations in the highlight region, but with the phase being 0° in the illuminated seafloor sector. Already at $L = 2$ the MVDR is able to greatly suppress noise. This is a common observation; adding a little flexibility to adapt to the scene has a dramatic effect, but further allowing full flexibility is much less significant. The media file also shows that MVDR can be run with subarray sizes $L \in [M/2, 5M/8]$, but only with temporal averaging $K = 1$ or above.

B. Kaiser parameter β and steering ϕ

To determine a suitable range for the Kaiser parameter β and steering ϕ , we constructed large and equally sized window databases containing Kaiser windows with varied upper boundaries for β and ϕ . The lower boundaries were chosen as $\beta = 0$ and $\phi = 0^\circ$, which includes the rectangularly weighted DAS image. The resulting images are shown in Fig. 4. In each image we computed the lateral distance Δx between the -3 dB points of the anchor, with the reference Δx_{ref} being the rectangularly weighted DAS image. A forth

order polynomial fit was used in this computation. This measure is also commonly called the full width half maximum (FWHM). In the case of imaging a point scatterer, it is closely related to the resolution of the system. For a rectangular window, for instance, the system resolution is approximately $\Delta \approx \text{FWHM}/0.89$ [9].

The LCA images in Fig. 4 demonstrate the effect of adjusting the upper bound of β and ϕ . As suggested by Fig. 3 we first attempted to use $\beta \in [0, 2]$. While this significantly improved sidelobe suppression, a slight further improvement was observed up to $\beta \in [0, 5]$. This can likely be explained by the need to compensate for the increased sidelobe levels caused by steering. No noticeable difference were observed for higher values than $\beta = 5$. The images also demonstrate that increasing the upper bound for steering ϕ improves the resolution of the strong scatterers. For this sonar the Rayleigh resolution is $\Delta \approx 0.0125$ radians (0.72°), so a point scatterer imaged at 19 m range with a rectangular DAS would have a lateral FWHM $\approx 0.125 \cdot 19 \text{ m} \cdot 0.89 = 21 \text{ cm}$. This is close to the FWHM of the anchor in the DAS image in Fig. 4, which means that the acoustic fingerprint of the anchor is similar to a point source. This suggests the anchor reflections to be specular and that we view its rounded side. As we increase steering to either 50% or 100% of the -3 dB width, the FWHM drops to 73% or 53% to that of the rectangular

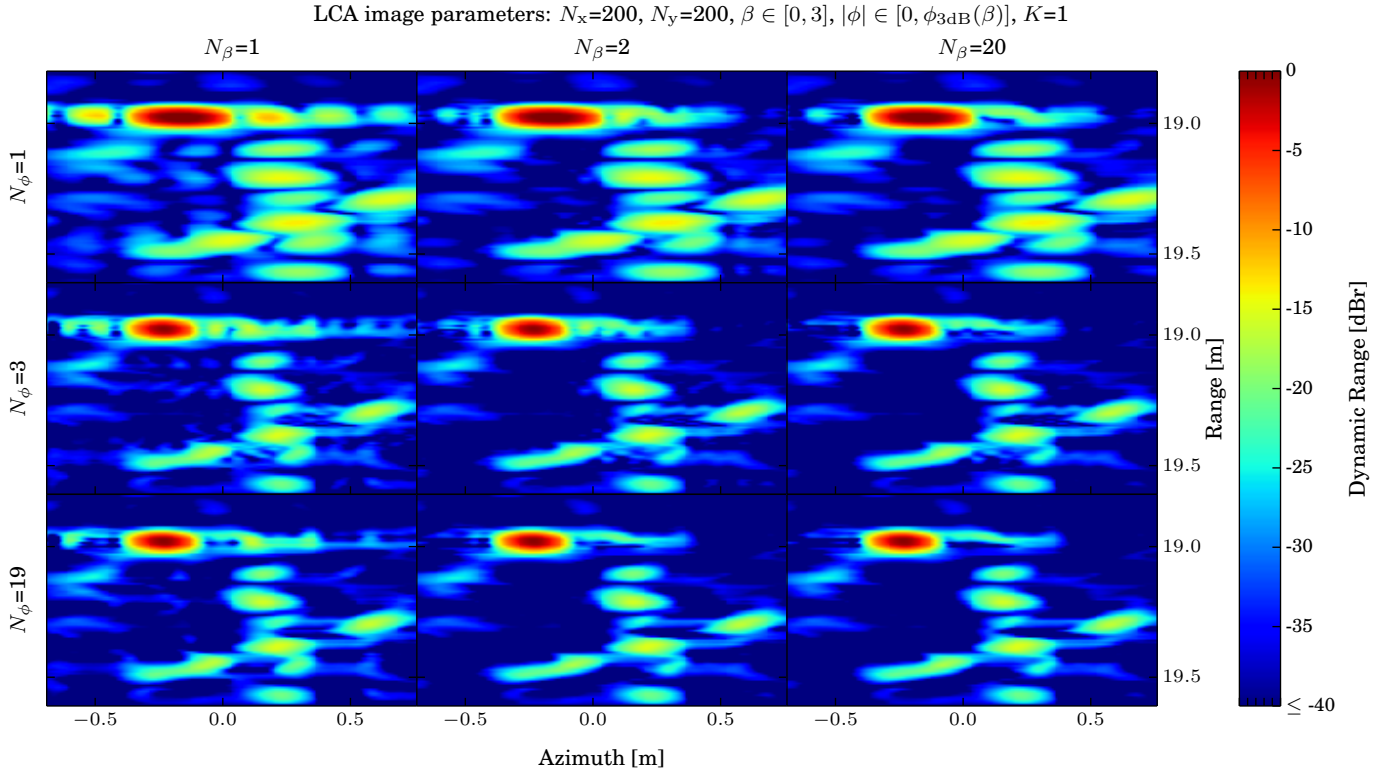


Fig. 6. LCA images using different window database sizes. The window boundaries are the same. The upper left image is identical to a rectangularly weighted DAS. Observe that sampling the β -range more finely increases the sidelobe suppression but leaves resolution unchanged. Adding more steering-variations improves both sidelobe suppression and resolution. However, using more than $N_\beta = 2$ window types and $N_\phi = 3$ steering angles makes minimal difference.

window, respectively.

Fig. 5a and Fig. 5b illustrates which β and ϕ values LCA prefers for different regions in the image of the cross. Red marker lines are used to pinpoint the cut line, location of the anchor and strong scatters on the cross. Observe that in the anchor region only narrow responses ($\beta = 0$) are used, which is the reason for the anchor FWHM being measured to the same value regardless of the upper bound of β in Fig. 4. On other scatterers with strong nearby lateral interference LCA prefers wider windows to suppress the interference. When allowed LCA prefers to steer windows away from the sources, but never exceed the $\phi_{3\text{dB}}(\beta)$ limit. When exceeding this bound we observed oscillation artifacts in the image.

C. Window database size

So far we have found it reasonable to use Kaiser windows in the range $\beta \in [0, 5]$, each steered within the range $|\phi| \in [0, \phi_{3\text{dB}}(\beta)]$. What remains is to determine the number of windows needed. We study this in Fig. 6, where we compared LCA images made from windows databases of different sizes, but with the same parameter boundaries. We included the results from using a single window ($N_\beta = 1$) and steering angle ($N_\phi = 1$), which corresponds to an unsteered rectangularly weighted DAS.

Observe that sampling the β -range more finely increases the sidelobe suppression but leaves resolution unchanged. Adding more steering-variations improves both sidelobe suppression and resolution. We can observe a major improvement going

to $N_\beta = 2$ and $N_\phi = 3$, but minimal improvement by adding yet more windows.

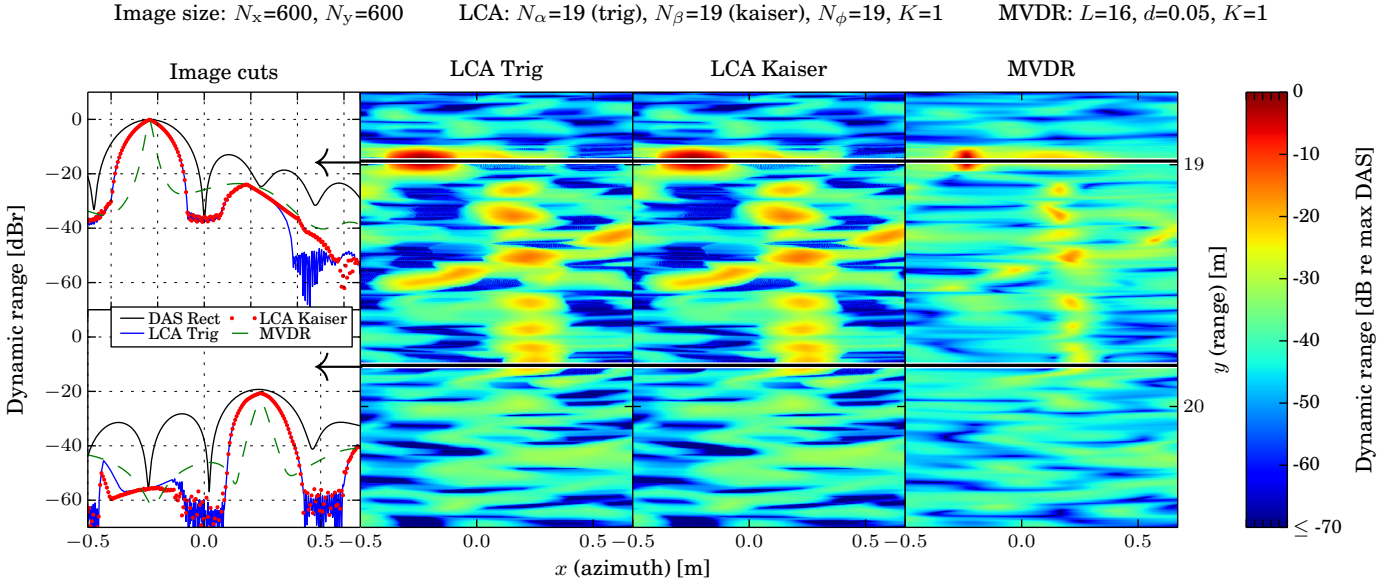
D. Image quality

We compare LCA image quality to that of DAS and MVDR in Fig. 7. In Fig. 7a we display the images computed by LCA using Kaiser windows, LCA using trigonometric windows, and MVDR. Two lateral image cuts through all images are presented in the left plot. The images and their corresponding cuts are near identical for the LCA version with Kaiser windows and the one with trigonometric windows. Compared to DAS the LCA produces targets with an FWHM that lies in between that of DAS and MVDR.

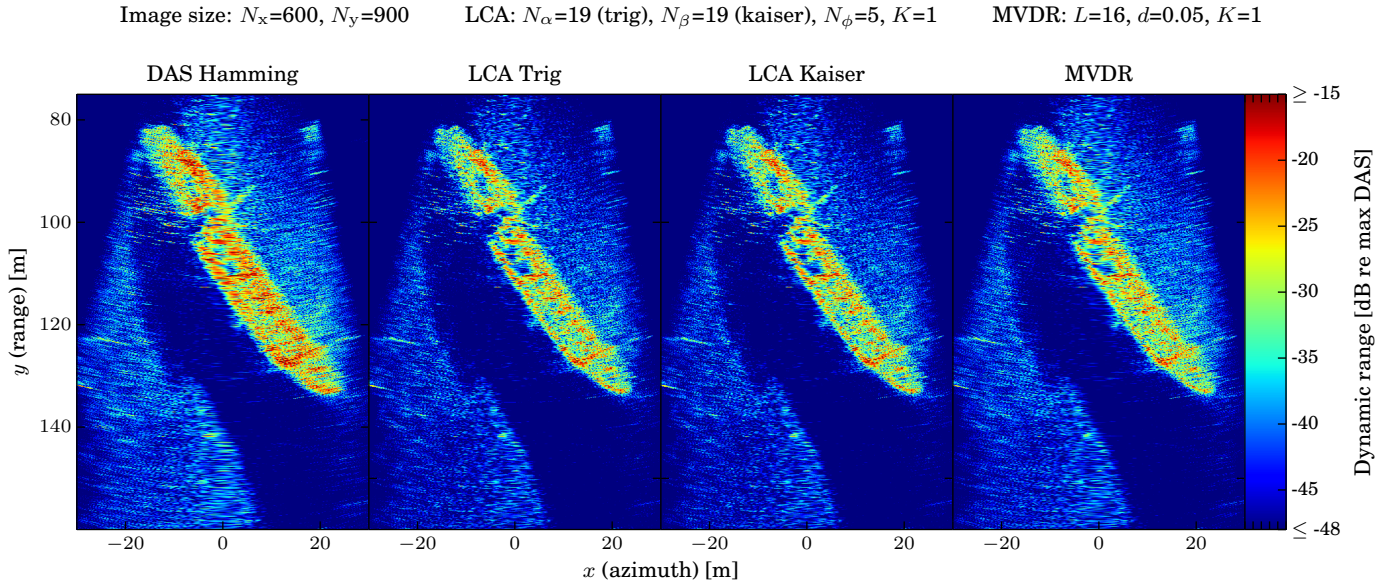
In Fig. 7b we show full sector images of the Holmengraa wreck. We compare the images produced by a Hamming weighted DAS, by MVDR and by LCA with Kaiser or trigonometric windows. All the adaptive beamformers produce a sharper and less noisy image than DAS, but the difference between LCA and MVDR is minimal. The LCA image produced with Kaiser windows appear identical to that from trigonometric windows.

E. Computational complexity

The computational complexity of MVDR is generally considered to be of $O(M^3)$. However, the implementation we are using is optimized so that building the spatial covariance matrix is of $O(N_k N_L L^2)$, and inverting it is of $O(L^3)$. We



(a) *Image quality of approximate point scatterers found in the cross scene.* Two lateral image cuts are shown in the leftmost figures, along with the response of a rectangularly weighted DAS. Note how the FWHM of LCA sits in between that of DAS and MVDR. Also note how LCA is insensitive to the window type; its performance is near identical whether it uses Kaiser or trigonometric windows.



(b) *Image quality of the full sector Holmengraa scene.* Compared to DAS the adaptive beamformers produce deeper shadows, sharper edges and a higher detail level. The adaptive methods produce nearly identical images.

Fig. 7. Comparing image quality of DAS, MVDR and LCA with Kaiser or trigonometric windows.

describe this implementation in [6], and a beamspace version in [7], where we optimize if for a graphics processing unit (GPU) for nearly two orders of magnitude speed increase compared to a straightforward C implementation. However, MVDR is not ideal for GPUs due to the complex data dependencies present in the covariance computation, and at best we only managed to utilize 10% of the GPUs potential.

In comparison, LCA is of $O(MN_\beta N_\phi)$, and extremely well suited for GPUs. Each pixel depends on only a small subset of data, and the windows can be precomputed and stored in GPU cache for near immediate access. If we use a trigonometric window function we solve for the window parameter analytically as described in appendix A. This reduces the complexity

to $O(MN_\phi)$, and the only remaining LCA parameter is the steering amount.

VI. CONCLUSION

LCA iterates through a set of windows in search of the one that minimizes the noise and interference power in each image pixel. It can be viewed as either a reduced solution space version of MVDR, or as an multi-taper extension to DAS. It creates images similar to MVDR, but at a fraction of the computational cost. It is also inherently robust and insensitive to the particular set of windows it selects from, supported by the observation that LCA can be used with either Kaiser or trigonometric windows and produce near identical images.

When using LCA with Kaiser windows we made their responses similar to those typically chosen by a robust MVDR in key areas in the image. We suggest an upper bound for β between 2 and 5, where 5 is slightly better at suppressing sidelobes. For ϕ we suggest to steer either to 50% or 100% of the -3 dB width, which leads to a resolution of 73% or 54% of the rectangular window, respectively. As lower boundaries we set $\beta = 0$ to always include a rectangular window, and $\phi = 0$ to always include the centered window.

The tendency of the LCA to perform similarly to the MV beamformer seems to indicate that a full solution space is rarely needed in real world scenarios.

APPENDIX A REDUCING LCA COMPLEXITY

Throughout this article we have used LCA with the Kaiser window function. However, as shown in Fig. 7 we can obtain similar performance using the trigonometric window function. For this window we can obtain an analytic solution for the optimal value of α in the minimum variance sense. To derive it, we start by inserting the trigonometric function (13), with applied steering (11), into the beamformer equation (1):

$$\begin{aligned} \mathbf{w}^H \mathbf{x} &= \sum_{m=0}^{M-1} [\mathbf{a}_\phi]_m \left(\alpha - (1-\alpha) \cos \left(\frac{2\pi m}{M-1} \right) \right) x_m^* \\ &= \alpha \mathbf{a}_\phi^T \mathbf{x} - (1-\alpha) \mathbf{b}_\phi^T \mathbf{x} \end{aligned} \quad (15)$$

where $[\mathbf{a}_\phi]_m$ is the m th component of the steering vector \mathbf{a}_ϕ defined in (11), and

$$\mathbf{b}_\phi = \text{diag}(\mathbf{a}_\phi) \cdot \begin{bmatrix} 1 & \cos \left(\frac{2\pi}{M-1} \right) & \cos \left(\frac{2\pi 2}{M-1} \right) & \dots & 1 \end{bmatrix}^T. \quad (16)$$

Unity gain in the look direction is ensured as long as the weights sum to one:

$$\mathbf{b}_\phi^T \mathbf{1} = (\alpha \mathbf{a}_\phi^T \mathbf{1} - (1-\alpha) \mathbf{b}_\phi^T \mathbf{1})^T \mathbf{1} = 1. \quad (17)$$

This is true for any value of α if $\mathbf{a}_\phi^T \mathbf{1} = 1$ and $\mathbf{b}_\phi^T \mathbf{1} = 1$. Hence, we preserve the unity gain constraint as long as we normalize \mathbf{a}_ϕ and \mathbf{b}_ϕ .

Now let $a = \mathbf{a}_\phi^T \mathbf{x}$ and $b = \mathbf{b}_\phi^T \mathbf{x}$. The beamformer output can then be written as:

$$\begin{aligned} |\mathbf{w}^H \mathbf{x}|^2 &= |aa - (1-\alpha)b|^2 \\ &= \alpha^2(aa^* + ab^* + a^*b + bb^*) \\ &\quad - \alpha(ab^* + a^*b + 2bb^*) + bb^* \end{aligned} \quad (18)$$

This is a convex function with a single minimum, which we find by differentiating with respect to α and setting equal to 0:

$$\begin{aligned} \frac{\partial}{\partial \alpha} |\mathbf{w}^H \mathbf{x}|^2 &= 2\alpha(aa^* + ab^* + a^*b + bb^*) \\ &\quad - (ab^* + a^*b + 2bb^*) = 0, \end{aligned} \quad (19)$$

which has the solution:

$$\alpha = \frac{ab^* + a^*b + 2bb^*}{2(aa^* + ab^* + a^*b + bb^*)}. \quad (20)$$

In this computation there are only 4 and 7 unique complex additions and multiplications, respectively. If we used this to analytically solve for α , but perform the search for ϕ , the computational complexity of LCA would be of $O(MN_\phi)$ instead of $O(MN_\alpha N_\phi)$. The solution for α would also yield the optimal beamformer output in the minimum variance sense.

ACKNOWLEDGMENT

The authors would like to thank Kongsberg Maritime, the Norwegian Defence Research Establishment (FFI), and Bundeswehr Technical Center for Ships and Naval Weapons, Maritime Technology and Research (TD 71), for the equipment and effort needed to acquire data of the and Holmengraa, as well as for allowing us to use it.

REFERENCES

- [1] J. Capon, "High-resolution frequency-wavenumber spectrum analysis," *Proceedings of the IEEE*, vol. 57, no. 8, pp. 1408–1418, 1969.
- [2] A. E. A. Blomberg, A. Austeng, R. E. Hansen, and S. A. V. Synnes, "Improving Sonar Performance in Shallow Water Using Adaptive Beamforming," *IEEE Journal of Oceanic Engineering*, vol. 38, no. 2, pp. 297–307, Apr. 2013.
- [3] A. E. A. Blomberg, A. Austeng, and R. E. Hansen, "Adaptive Beamforming Applied to a Cylindrical Sonar Array Using an Interpolated Array Transformation," *IEEE Journal of Oceanic Engineering*, vol. 37, no. 1, pp. 25–34, Jan. 2012.
- [4] S. D. Han, A. Austeng, R. E. Hansen, and S. Holm, "Minimum variance beamforming in active sonar imaging," in *Proceedings of the 3rd International Conference & Exhibition on Underwater Acoustic Measurements: Technologies and Results*, B. r. e. John S. Papadakis & Leif, Ed., 2009, pp. 1373–1378.
- [5] K. Lo, "Adaptive Array Processing for Wide-Band Active Sonars," *IEEE Journal of Oceanic Engineering*, vol. 29, no. 3, pp. 837–846, Jul. 2004.
- [6] J. I. Buskenes, J. P. Asen, C.-I. C. Nilsen, and A. Austeng, "An Optimized GPU Implementation of the MVDR Beamformer for Active Sonar Imaging," *IEEE Journal of Oceanic Engineering*, pp. 1–13, 2014.
- [7] J. P. Åsen, J. I. Buskenes, C.-I. Colombo Nilsen, A. Austeng, and S. Holm, "Implementing capon beamforming on a GPU for real-time cardiac ultrasound imaging," *IEEE transactions on ultrasonics, ferroelectrics, and frequency control*, vol. 61, no. 1, pp. 76–85, Jan. 2014.
- [8] J.-F. Synnevåg, S. Holm, and A. Austeng, "A low complexity data-dependent beamformer," in *2008 IEEE Ultrasonics Symposium*, no. 2. IEEE, Nov. 2008, pp. 1084–1087.
- [9] F. Harris, "On the use of windows for harmonic analysis with the discrete Fourier transform," *Proceedings of the IEEE*, vol. 66, no. 1, pp. 51–83, 1978.
- [10] T. Kailath and T.-J. Shan, "Adaptive beamforming for coherent signals and interference," *IEEE Transactions on Acoustics, Speech, and Signal Processing*, vol. 33, no. 3, pp. 527–536, Jun. 1985.
- [11] J.-F. Synnevåg, A. Austeng, and S. Holm, "Benefits of minimum-variance beamforming in medical ultrasound imaging," *IEEE Transactions on Ultrasonics, Ferroelectrics and Frequency Control*, vol. 56, no. 9, pp. 1868–1879, Sep. 2009.
- [12] H. Cox, R. Zeskind, and M. Owen, "Robust adaptive beamforming," *IEEE Transactions on Acoustics, Speech, and Signal Processing*, vol. 35, no. 10, pp. 1365–1376, Oct. 1987.
- [13] J. N. Maksym, "A robust formulation of an optimum cross-spectral beamformer for line arrays," *The Journal of the Acoustical Society of America*, vol. 65, no. 4, p. 971, 1979.
- [14] J. P. Åsen, A. Austeng, and S. Holm, "Capon beamforming and moving objects—an analysis of lateral shift-invariance," *IEEE transactions on ultrasonics, ferroelectrics, and frequency control*, vol. 61, no. 7, pp. 1152–60, Jul. 2014.
- [15] R. E. Hansen, H. J. Callow, T. O. Sæbø, S. A. Synnes, P. E. Hagen, G. Fossum, and B. Langli, "Synthetic aperture sonar in challenging environments: Results from the HISAS 1030," in *Proceedings of the 3rd International Conference & Exhibition on Underwater Acoustic Measurements: Technologies and Results*, 2009.
- [16] Article of Holmengraa on dykkepedia.com.



Jo Inge Buskenes received the B.Sc. degree in electrical engineering from Gjøvik College University, Norway, in 2007, and the M.Sc. degree in instrumentation for particle physics from the University of Oslo, Norway, in 2010. He is currently pursuing the Ph.D. degree in image reconstruction and technology at the University of Oslo.

His industry experience includes the European Organization for Nuclear Research (CERN), Geneva, Switzerland (2007-2008), and the Norwegian Defence Research Establishment, Kjeller, Norway (2009). He has lectured in digital signal processing at the Gjøvik College University (2009), and at the University of Oslo (2010-2013). His research interests include adaptive beamforming, digital image reconstruction, high performance computing, intelligent detector design and open source software.



Roy Edgar Hansen (M'07) received the M.Sc. and Ph.D. degrees in physics from the University of Tromsø, Tromsø, Norway, in 1992 and 1999, respectively.

From 1992 to 2000, he was with the Norwegian research company TRIAD, working on multistatic sonar, multistatic radar, synthetic aperture radar (SAR), and underwater communications. Since 2000, he has been with the Norwegian Defence Research Establishment (FFI), Kjeller, Norway. He is currently Principal Scientist and team leader for the autonomous underwater vehicle development and the synthetic aperture sonar development at FFI. He is also Adjunct Associated Professor at the [Centre for Imaging](#), University of Oslo, Oslo, Norway.



Andreas Austeng was born in Oslo, Norway, in 1970. He received the M.Sc. degree in physics in 1996 and the Ph.D. degree in computer science in 2001, both from the University of Oslo. Since 2001, he has been working at the Department of Informatics, University of Oslo, first as a postdoctoral research fellow and currently as an associate professor. His research interests include signal and array processing for acoustical imaging.